

curved water surface will be equal to

$$p_{\text{sat}} = p_{\text{sat}}^0 \exp(-v_0 p_{\text{cl}} / kT), \quad (20)$$

where v_0 is the volume per water molecule in the water phase, k is Boltzmann's constant, T is the absolute temperature, and p_{sat}^0 is the saturation pressure over the plane surface. Substituting (6) in (20), we obtain

$$p_{\text{sat}} = p_{\text{sat}}^0 \exp\left(-\frac{v_0 K}{kT} \frac{\Delta V_s}{V_s}\right). \quad (21)$$

Equation (21) connects the equilibrium saturated-vapor pressure with the degree of dehydration of the protein crystal. It follows from (21) that to each saturated vapor pressure p_{sat} there corresponds an equilibrium degree of dehydration of the protein crystal, equal to

$$\frac{\Delta V_s}{V_s} = \frac{kT}{Kv_0} \ln \frac{p_{\text{sat}}}{p_{\text{sat}}^0}. \quad (22)$$

It should be kept in mind that the relation (22) describes the degree of dehydration of the crystal only so long as no conformational changes of the globule, polymorphic transformations, or boiling and loss of stability of the water film relative to the Laplace pressure take

place. All the enumerated processes offset the change in the Laplace pressure and should lead to the appearance of plateaus on the dehydration curves.

¹In the one-dimensional case, a similar problem arises in the calculation of the critical stress necessary for the extrusion of a dislocation line between pinning points (theory of precipitation hardening).^[3]

²This effect has been observed in particular in crystals of gramicidine.^[6,7]

³M. F. Perutz, *Trans. Faraday Soc.* **B42**, 187 (1946).

⁴F. M. Richards, *Ann. Rev. Biochem.* **32**, 278 (1963).

⁵E. Orovan, *Symposium on Internal Stresses*, London, 1947.

⁶A. G. Pasynskii, *Belki i ikh spetsificheskie svoïstva* (Proteins and their Specific Properties), Ukrainian Acad. Sci. Press, 1955.

⁷D. S. Chernavskii, Yu. I. Khurin and S. E. Shnol', *Molek. Biol.* **1**, 413 (1967).

⁸G. N. Tishchenko, K. A. Zykalo and I. A. Silant'eva, *Kristallografiya* **9**, 37 (1964) [*Sov. Phys. Crystallography* **9**, 26 (1964)].

⁹G. N. Tishchenko, K. A. Zykalo and A. I. Grebenko, *Kristallografiya* **12**, 868 (1967) [*Sov. Phys. Crystallography* **12**, 758 (1968)].

Translated by R. T. Beyer

Gas-liquid phase diagram in a nonequilibrium electron-hole system in silicon

A. F. Dite, V. D. Kulakovskii, and V. B. Timofeev

Institute of Solid State Physics, USSR Academy of Sciences

(Submitted September 19, 1976)

Zh. Eksp. Teor. Fiz. **72**, 1156–1170 (March 1977)

We investigate the condensation of high-density excitons and nonequilibrium carriers, produced by intense optical pumping at low temperatures, into drops of electron-hole liquid. The phase diagram of the gas-liquid transition is plotted in coordinates n and T (density and temperature) on the basis of an analysis of the shapes of the recombination-radiation spectra and of the kinetics of their evolution in time. The principal thermodynamic characteristics are determined, as well as the temperature dependences of the chemical potential, of the density, and of the Fermi energies in the liquid phase. The critical parameters $n_c = (1.2 \pm 0.2) \times 10^{18} \text{ cm}^{-3}$ and $T_c = (28 \pm 2) \text{ K}$ are obtained. It is shown that at an average density $n = (5 \pm 3) \times 10^6 \text{ cm}^{-3}$ the dielectric exciton gas is transformed into a metallic electron-hole plasma.

PACS numbers: 71.35.+z, 64.70.Fx

1. INTRODUCTION

At low temperatures, an exciton gas of sufficiently high density in semiconductors can become condensed into drops of an electron-hole liquid (EHL).^[1] The region of existence of electron-hole drops (EHD) can be obtained from the n - T phase diagram, in which the gas-liquid equilibrium curve is determined on the gas-phase side by the singularities of the kinetics of exciton condensation, and on the side of the liquid phase by the internal properties of the EHL. We point out here a singularity that should be possessed by the gas-liquid phase

transition in a high-density system of excitons (or nonequilibrium carriers). It turns out that the density of the nonequilibrium $e-h$ pairs in the liquid is $n_c > n_{MI}$, where n_{MI} is the density at which the "metallization" of the excitons takes place. Therefore at average densities $\bar{n} < n_{MI}$ a dielectric exciton gas condenses into EHL drops whereas at $n_c > \bar{n} > n_{MI}$ a gas of metallic electron-hole plasma (EHP) should be condensed. Thus, the gas-liquid coexistence curve (at $\bar{n} \sim n_{MI}$) has a region in which the exciton gas is transformed into a metallic EHP. What is still in question is whether this transformation is analogous in character to a first-order phase transition.

We investigate in this paper the gas-liquid phase diagram in a nonequilibrium electron-hole system in silicon, including the region close to critical. The carrier density n_0 in the liquid phase, the electron temperature, and also the threshold values of the saturated vapor density of the gas, at which condensation into liquid sets in, are determined on the basis of an analysis of the shapes of the recombination-radiation (RR) spectra and their kinetics (Sec. 3). The equilibrium curve on the liquid-phase side is plotted and the principal thermodynamic quantities characterizing the EHL are determined (Secs. 4 and 5). The gas-liquid coexistence curve (on the gas-phase side) is determined from threshold measurements of the saturated-vapor density of the gas, and it is shown that at $\bar{n} > (5 \pm 3) \times 10^{16} \text{ cm}^{-3}$ the exciton gas is transformed into an EHP (Sec. 6). Within the limits of the experimental accuracy, we have observed no spectroscopic singularities indicating that such a "metallization" of the excitons is the consequence of a first-order phase transition.

2. EXPERIMENTAL TECHNIQUE AND CRYSTALS

To investigate the n - T (density-temperature) phase diagram in a nonequilibrium electron-hole system in silicon it is necessary to use rather powerful radiation sources that produce electron-hole ($e-h$) pair concentrations \bar{n} (averaged over the volume) up to $\bar{n} \approx 2 \times 10^{18} \text{ cm}^{-3}$ near the critical temperature T_c . We have used in this study both continuous and pulsed excitation sources.

The continuous radiation source was a DKSSh-1000 high-pressure xenon lamp. Filters were used to vary the radiation in the spectral range 0.7-1.0 μm . The use of a conical light pipe with such a source provided a power density up to $P = 30 \text{ W/cm}^2$ ($\bar{n} \sim 3 \times 10^{16} \text{ cm}^{-3}$) at an excitation-spot dimension on the sample of approximately 3 mm^2 .

For pulsed excitation we used a copper-vapor laser with the following parameters: power and duration of a single pulse 10 kW and 10 nsec, respectively, pulse repetition frequency 10 kHz, and lasing wavelength 5105 \AA .

The RR receiver was a photomultiplier, cooled to $t = -60^\circ\text{C}$, with a cathode of S-1 type, for which the photon-counting regime could be realized. When operating at constant excitation, the RR of the sample was interrupted at a frequency 180 Hz, and was registered in the synchronous-detection regime. In the case of excitation by a pulsed laser, we used a registration system operating in the strobe-integration regime. The strobe duration could be adjusted in the range 0.1-5 μsec , and the delay of the strobe relative to the excitation pulse could be continuously varied from 0 to 50 μsec . In the experiment, the duration of the strobing pulse was chosen to be shorter than the characteristic recombination time. The threshold sensitivity of the receiver was 10^{-13} W . The spectral instrument was a double diffraction monochromator with dispersion 10 $\text{\AA}/\text{mm}$ in the operating range.

We used in the investigation single crystals of pure

silicon (the concentration of the residual electrically active impurities was $n_{d,a} < 5 \times 10^{12} \text{ cm}^{-3}$) in the form of thin plates ($d \sim 30 \mu\text{m}$) or bulky samples in the form of Weierstrass spheres ($\sim 5 \text{ mm}$ diameter). Before they were placed in the cryostat, the samples were etched in a mixture of fluoric and nitric acids (1:3). The work was performed with the samples placed either directly in the liquid helium or (for measurements at high temperatures) in its vapor. At $T > 5 \text{ K}$, the temperature in the cryostat was stabilized accurate to 0.1 K.

At high pump densities ($\geq 10^{16} \text{ cm}^{-3}$), the temperature in the excited region of the crystal was always higher than the temperature of the thermostat (T_{therm}). The temperature of the nonequilibrium electron-hole system was therefore monitored in the experiment directly against the shape of the exciton-phonon recombination spectrum. In particular, at $T < 8 \text{ K}$, when the exciton-phonon spectrum broadening Γ due to the nonstationary character of the exciton decay processes was predominant ($\hbar\Gamma \geq kT$), the exciton temperature was estimated, following^[2], from the ratio of the intensities of the TO and LO components of the exciton-phonon spectrum. At $T > 8 \text{ K}$, when $\hbar\Gamma < kT$, the temperature was determined from the shape of the exciton-phonon spectrum, which is described satisfactorily, up to $T \sim 80 \text{ K}$ and at average concentrations $\sim 5 \times 10^{16} \text{ cm}^{-3}$, by the expression

$$I(\epsilon) \sim \epsilon^{\hbar\Gamma} \exp(-\epsilon/kT), \quad (1)$$

which indicates a Boltzmann exciton distribution in the band (ϵ is the energy of the exciton motion, reckoned from the "red" boundary of the exciton-phonon spectrum). The sensitivity of the apparatus made it possible to record the recombination radiation of the excitons with a resolution 0.2 meV. The error in the determination of the exciton temperature did not exceed in this case 1.5 K.

We note that in bulky Si samples ($5 \times 5 \times 5 \text{ mm}$) placed in liquid-helium vapor, under pulsed excitation by $\bar{n} \sim 10^{18} \text{ cm}^{-3}$ $e-h$ pairs, the heat rise $T_{\text{ex}} - T_{\text{therm}}$ amounted to 6 degrees. Under stationary excitation at $\bar{n} \sim 3 \times 10^{16} \text{ cm}^{-3}$, the difference $T_{\text{ex}} - T_{\text{therm}}$ reached 12 degrees for bulky samples placed directly in the liquid helium. Other conditions being equal, the heat rise of thin samples was always substantially larger.

3. KINETICS OF SHAPES OF THE RECOMBINATION RADIATION SPECTRA AT VARIOUS TEMPERATURES

We investigated the shapes of the recombination-radiation spectra of silicon, as well as the kinetics of the shapes of the spectra at different excitation densities up to $2 \times 10^{15} \text{ cm}^{-3}$ in the temperature interval 2-80 K. On the basis of the time behavior of the spectrum shape, it is expedient to distinguish between three temperature regions.

1. $T \leq 18 \text{ K}$ ($\bar{n} < 2 \times 10^{17} \text{ cm}^{-3}$). In this temperature interval one observes distinctly two emission bands corresponding to the EHD and to the gas of free electrons. The EHD band appears in the spectrum only after the nonequilibrium $e-h$ pairs reach the threshold density,

and this threshold rises steeply with increasing temperature. For example, at 2 and 18 K the threshold values of the average density are $\sim 3 \times 10^{14}$ and $\sim 3 \times 10^{16}$ cm^{-3} , respectively. The most characteristic feature of this temperature interval is that the EHD and exciton bands are distinctly separated, and each has its own damping time that does not depend on the wavelength within the limits of the corresponding band. Figures 1a and 1b show the kinetics of the shapes of the recombination-radiation spectra of the EHD and of the excitons at 4.5 and 16 K, obtained at different delays relative to the excitation pulse. For convenience in the comparison, the spectra are normalized to the maximum of the EHD band. When the radiation intensity of the EHD is attenuated within two orders of magnitude, at a fixed temperature, the shape of the recombination spectrum remains unchanged. With increasing temperature, the EHD band becomes more symmetrical on account of the broadening of the "violet" part of the spectrum, in accordance with the temperature spreading of the Fermi distribution functions in the electron and hole bands. The temperature dependence of the shape of the exciton-phonon spectrum is well approximated by expression (1), in agreement with the quasi-equilibrium distribution of the excitons. When the temperature is raised from 2 to 18 K, the damping time τ_{EHD} decreases within the

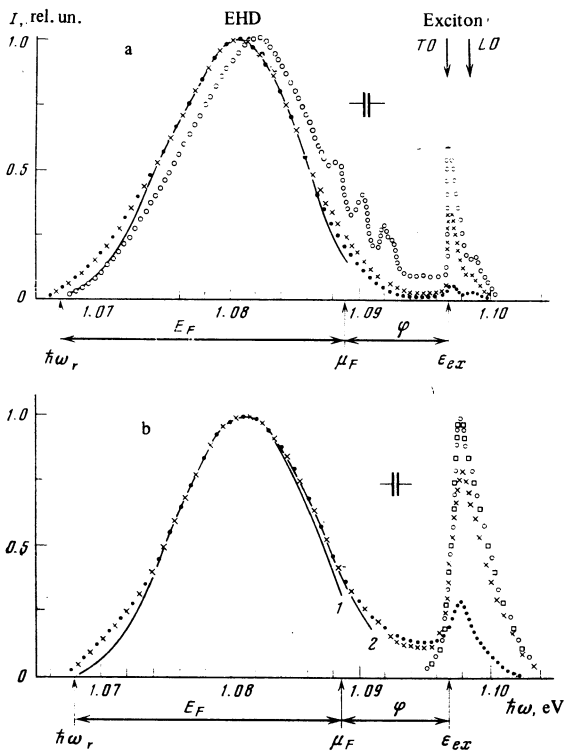


FIG. 1. Kinetics of the shape of the recombination-radiation spectrum of silicon at $\bar{n} \approx 1.5 \times 10^{18} \text{ cm}^{-3}$. Points—experiment, delay τ relative to the excitation pulse in microseconds, gain τ : a) $T = 4.5 \text{ K}$, \bullet — $0.1 \mu\text{sec}$ ($\times 1$), \times — $1 \mu\text{sec}$ ($\times 50$), \circ —stationary excitation; b) $T = 16 \text{ K}$, \bullet — $0.1 \mu\text{sec}$ ($\times 1$), \times — $0.6 \mu\text{sec}$ ($\times 9$), \circ — $1.6 \mu\text{sec}$ ($\times 13$), \square — $3.2 \mu\text{sec}$ ($\times 16$). Solid lines—calculation of the shape of the EHD spectrum at: c) $n_0 = 3.35 \cdot 10^{18} \text{ cm}^{-3}$; $T = 4.5$; d) $n_0 = 3.1 \cdot 10^{18} \text{ cm}^{-3}$, $T = 16 \text{ K}$ (curve 1), $T = 19 \text{ K}$ (curve 2).

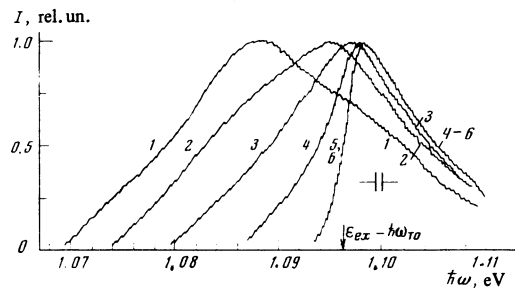


FIG. 2. Kinetics of shapes of RR spectra of silicon at 50 K and $\bar{n} = 1.5 \times 10^{18} \text{ cm}^{-3}$. Spectra 1–6 were obtained with delays of 0, 0.5, 1.5, 3, 7, and 15 μsec , respectively.

limits of the EHD band from 0.25 ± 0.05 to $0.20 \pm 0.05 \mu\text{sec}$, while the damping time of the exciton band τ_{ex} increases from 1.5 ± 0.3 to $6 \pm 0.5 \mu\text{sec}$.

In the recombination radiation spectra of the same sample, measured under stationary-excitation conditions at $T < 8 \text{ K}$ and $\bar{n} < 10^{16} \text{ cm}^{-3}$, narrow lines are observed, due according to [3, 4] to the emission of many-particle exciton-impurity complexes (in our case, excitons bound to boron atoms). It should be noted that at helium temperatures the EHD spectrum is shifted under pulsed excitation towards lower energies by approximately 1 meV in comparison with the analogous spectrum obtained under stationary pumping conditions. This spectral shift practically vanishes. The reason for this difference between the positions of the spectra may be that at relatively weak stationary pumping the EHD are generated in crystal regions where the impurity concentration is larger. A similar shift of the EHD line is observed in doped silicon crystals, and the magnitude of the shift depends on the concentration and on the type of the impurity. [5]

2. $T > 30 \text{ K}$. Judging from the emission spectra of silicon at $T > 30 \text{ K}$, the entire investigated pump region, up to $\bar{n} = 2 \times 10^{18} \text{ cm}^{-3}$, contains no noticeable singularities attesting to condensation of the nonequilibrium $e-h$ pairs and of the excitons into EHD. Only one band is observed in all the recombination spectra in this temperature region. Similar radiation-recombination spectra in silicon were observed in [6] at 80 K. At relatively small pumps, $\bar{n} < 3 \times 10^{16} \text{ cm}^{-3}$, the observed band corresponds to exciton emission: it has an asymmetric shape typical of the exciton-phonon spectrum, with a distinct "red" boundary and a single damping time independent of n within the entire spectrum, and is on the whole satisfactorily described by expression (1) at each specified value of T . The value of τ_{ex} decreases with increasing temperature, from $5 \pm 0.5 \mu\text{sec}$ at 28 K to $3 \pm 0.5 \mu\text{sec}$ at 40 K.

Starting with $\bar{n} \sim 10^{16} \text{ cm}^{-3}$, the exciton-phonon spectrum broadens towards lower energies on account of the smearing of the "red" boundary. At $n = (1-3) \times 10^{16} \text{ cm}^{-3}$, this behavior can still be connected with the exciton-exciton (electron) collisions, which lead to an increase of the effective damping Γ and, consequently, to a more symmetrical shape of the curve. However, the reversal of the asymmetry sign at $\bar{n} > 5 \times 10^{16} \text{ cm}^{-3}$

cannot be attributed to collision processes. At $\bar{n} > 5 \times 10^{16} \text{ cm}^{-3}$ the behavior of the recombination radiation spectrum corresponds to EHP emission. With increasing density, up to $2 \times 10^{18} \text{ cm}^{-3}$, the "red" boundary of the recombination spectrum moves towards lower energies in accordance with the restructuring of the energy spectrum of the EHP because of the exchange and correlation interactions in the high-density electron-hole system.^[7] With increasing n , the width of the recombination spectrum of the EHP increases in accordance with the Fermi character of the filling of the electron and hole bands with carriers.

An example of the time evolution of the recombination radiation spectrum of EHP under pulsed excitation at an $e-h$ pair density $\sim 1.5 \times 10^{18} \text{ cm}^{-3}$ is shown in Fig. 2. Spectra 2-6 were obtained with different delays relative to the exciting pulse at a strobe duration 0.1 μsec . Each spectrum corresponds to a separate instantaneous value of the average density of the $e-h$ pairs. The damping time of the EHP emission line decreases monotonically with increasing wavelength and depends on \bar{n} . With decreasing \bar{n} , the EHP spectra (spectra 1-4 in Fig. 2) become narrower and their "red" boundary shifts towards higher energies. Only at $\bar{n} < 3 \times 10^{16} \text{ cm}^{-3}$ is the emission band converted into the exciton band and has a single damping time over the entire width of the exciton-phonon spectrum (spectra 5 and 6 of Fig. 2, which correspond to $\bar{n} \sim 10^{16}$ and $\bar{n} \sim 10^{15} \text{ cm}^{-3}$, have identical shapes).

Thus, it follows from the investigation of the recombination radiation spectra that the conversion of the exciton gas into an electron-hole plasma takes place in silicon at $\bar{n} = (5 \pm 3) \times 10^{16} \text{ cm}^{-3}$. The cause of this transition is the vanishing of the bound exciton states as a result of screening of the Coulomb interaction. According to^[8] this transition should take place when the screening radius is $r_{\text{scr}} = 0.84 a_B$, which in the case of a nondegenerate gas corresponds to a density

$$n_{MI}(T) = kT / 11.2 E_{ex} a_B^3, \quad (2)$$

where a_B is the radius of the Bohr orbit and E_{ex} is the binding energy of the exciton. The $n_{MI}(T)$ dependence calculated for silicon from formula (2) is given below (curve 3 of Fig. 4b). At $\bar{n} < n_{MI}$, owing to the screening of the Coulomb interaction, the bound exciton states vanish. It was suggested in^[9] that the transition of the dielectric exciton gas into a metallic electron-hole plasma can be of first order. An analogous transition in the case of a plasma was considered earlier in^[10]. According to the calculations of^[11] it follows, for example, that in Ge crystals, in a certain temperature region ($T < 10 \text{ K}$), an exciton gas with density \bar{n} close to n_{MI} should be unstable. This instability leads to a stratification of the system into regions occupied by a strongly ionized gas with large density $n \sim n_{MI} > \bar{n}$ and by a weakly ionized gas with $n < \bar{n}$. Our value of \bar{n} , at which metallization of the excitons takes place, agrees with that calculated from formula (2). We did not observe in our study any spectroscopic manifestations attesting to an instability near n_{MI} . Such an instability could hardly be revealed at all by the emission spectra

if the components of the stratified system remain non-degenerate gases, since, as follows from the measured recombination radiation spectra, the emission band of a nondegenerate electron-hole plasma gas with a density close to n_{MI} is located at practically the same position in the spectrum as the exciton band.

3. $20 \text{ K} < T < 27 \text{ K}$. The recombination radiation spectra of silicon reveal two bands in the temperature interval $20 \text{ K} < T < 27 \text{ K}$ and at densities $\bar{n} > 10^{17} \text{ cm}^{-3}$, indicating stratification of the crystal volume into regions occupied by the EHD and by the gas that surrounds them (Fig. 3). The overlap of these bands in the spectrum increases with increasing temperature. The EHD band is produced when a certain threshold is reached. This threshold increases with increasing temperature and reaches $\sim 5 \times 10^{17} \text{ cm}^{-3}$ at $T = 26 \text{ K}$. The damping time of the radiation remains constant only within the limits of the long-wave region of the EHD spectrum, which does not overlap the recombination spectrum of the gas phase. At $T = 25 \text{ K}$ we have $\tau_{EHD} = (0.3 \pm 0.1) \text{ sec}$.

The overlap of the emission bands of the EHD and of the gas phase in this temperature interval greatly complicates the subsequent analysis of the shapes of the spectra. This difficulty can be overcome, however, by using the difference between the damping times of

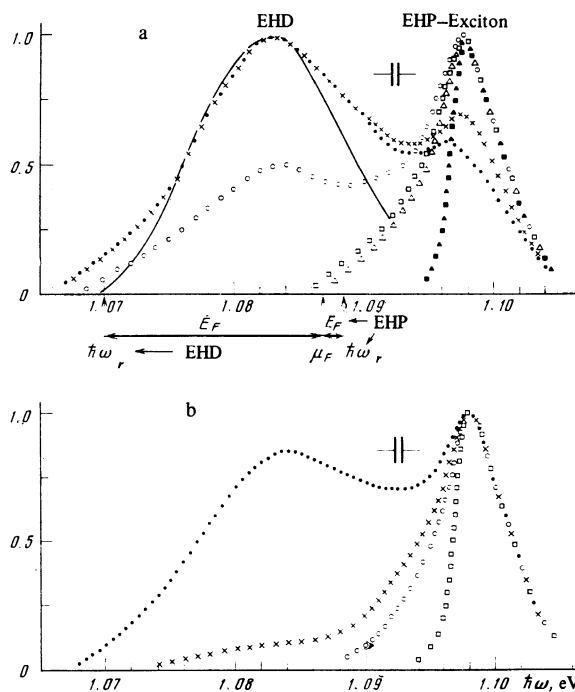


FIG. 3. a) Kinetics of the shape of the recombination radiation of silicon at 25 K and $\bar{n} \approx 1.5 \times 10^{18} \text{ cm}^{-3}$. Points—experiment, delay τ in μsec , gain (\times); \bullet —0.1 μsec ($\times 1$), \times —0.4 μsec ($\times 4$), \circ —0.7 μsec ($\times 6$), \square —1.2 μsec ($\times 6.5$), \triangle —1.4 μsec ($\times 6.8$), \blacktriangle —3.2 ($\times 9$), \blacksquare —4.8 μsec ($\times 12$). Solid-line calculation of the shape of the EHD spectrum at $n_0 = 2.5 \times 10^{18} \text{ cm}^{-3}$ and $T = 25 \text{ K}$. b) Dependence of the shape of the recombination radiation spectrum of silicon at $T = 25 \text{ K}$ on the excitation level. The experimental points correspond to an average density $4 \cdot 10^{17}$ (\bullet), $2.5 \cdot 10^{17}$ (\times), $1.5 \cdot 10^{17}$ (\circ) and $0.4 \cdot 10^{17}$ (\square) cm^{-3} .

the EHD and gas-phase bands, which reaches one order of magnitude, and if we investigate the time evolution of the shape of the spectrum under pulsed excitation. Figure 3a shows recombination spectra obtained at $T = 25$ K with different delays relative to an excitation pulse that generates $\bar{n} \sim 10^{18} \text{ cm}^{-3}$. It is seen that the intensity of the EHD band is the fastest to attenuate, and no traces whatever of this band remain in the spectrum already after 1 μsec .

At a delay of 1 μsec , there is still no time for noticeable changes to take place in the spectrum of the gas phase. This spectrum constitutes a broad (compared with the spectrum of the free excitons) band corresponding to the electron-hole plasma. With increasing delay, the emission spectrum of the electron-hole plasma becomes narrower, and its "red" boundary shifts toward higher energies. Only starting with delays $\tau_d \sim 3 \mu\text{sec}$, when the average density of the $e-h$ pairs reaches $\sim 10^{16} \text{ cm}^{-3}$, does the emission spectrum of the gas phase coincide fully with the exciton-phonon spectrum.

Thus, in this temperature interval, the electron-hole liquid seems to condense into drops directly from the gas of the non-equilibrium electron-hole plasma. This means that if the density \bar{n} is increased and the temperature is kept constant in the range $20 \text{ K} < T < 27 \text{ K}$, then at first, at $\bar{n} \sim 5 \times 10^{16} \text{ cm}^{-3}$, the dielectric exciton gas becomes "metallized" and is transformed into an electron-hole plasma, (EHP) after which, at certain threshold values of the density, a first-order phase transition takes place in the EHP-EHL system.

4. LIQUID-GAS EQUILIBRIUM REGION ON THE LIQUID-PHASE SIDE

To construct the liquid-gas coexistence curve on the liquid-phase side, we measured carefully the shape of the recombination spectrum of the EHD at different pumps and temperatures, after which, by analyzing the shape of the spectrum, we obtained the electron temperature T_{EHD} and the carrier density n_0 in the EHD.

1. At $T < 20$ K the emission spectra of the EHD and of the exciton gas are distinctly separated, so that T_{EHD} and n_0 were determined independently from the shape of the EHD spectrum^[7, 12] with sufficient accuracy. The spectral distribution of the recombination radiation of the EHD with emission of $\hbar\Omega^{\text{TO}}$ and $\hbar\Omega^{\text{LO}}$ phonons, under conditions of quasi-equilibrium, is described by the expression^[7]

$$I(\hbar\nu) = \int_0^{\hbar\nu} \frac{\epsilon^{\frac{1}{2}}(\epsilon - \hbar\nu)^{\frac{1}{2}} d\epsilon}{[1 + \exp((\epsilon - \epsilon_F^e)/kT)][1 + \exp((\hbar\nu - \epsilon - \epsilon_F^h)/kT)]}, \quad (3)$$

where $\epsilon_F^e(n_0, T)$ and $\epsilon_F^h(n_0, T)$ are the Fermi quasilevels of the electrons and holes at the temperature T . The energy $\hbar\omega$ of the emitted photon is

$$\hbar\omega = \hbar\nu + E_g - \epsilon_{\text{xc}} - \hbar\Omega,$$

where E_g is the width of the forbidden gap and ϵ_{xc} is the sum of the exchange and correlation energies. Expression (3) is valid in an approximation in which one neglects

the dependences of the instant of the optical transition and of the value of ϵ_{xc} on the quasimomentum (the latter means that one ignores the corrections to the kinetic energy of the electrons and holes, which depend on the quasimomentum and are due to the interparticle interactions). It is seen from (3) that n_0 and T are independent parameters that determine the shape of the spectrum.

When the experimental curve was approximated with the aid of expression (3), we took into account also the fact that the recombination radiation band of the EHD in silicon is a superposition of two rather broad bands with emission of TO (strong component) and LO (weak component) phonons; the components have an intensity ratio 10 : 1 at the maximum and are shifted in energy by $\hbar\Omega^{\text{TO}} - \hbar\Omega^{\text{LO}} = 1.8 \text{ meV}$.^[2] We note, however, that allowance for the contribution made to the system by the emission of the LO phonon alters the resultant value of n_0 by not more than 2%.

Figure 1 shows an approximation of the shapes of the recombination spectra of the EHD, obtained with the aid of expression (3) under conditions of pulsed excitation. The approximating curves were calculated with a computer. The arrows on the figure indicate the "red" boundaries $\hbar\omega_r$ and ϵ_{xc} of the recombination spectra of the electron hole drops and excitons, respectively, and also the chemical potential μ_F per pair of particles in the EHD, accurate up to the energy of the TO phonon. The greatest discrepancy between experiment and calculation is observed near the "red" boundary of the EHD spectrum. This smearing of the "red" boundary of the EHD spectrum, which was noted also earlier in^[7, 12, 13], is possibly due to the "tails" of the state densities of the allowed bands.

In the temperature interval $8 \text{ K} < T < 20 \text{ K}$, the error in the determination of T_{EHD} does not exceed 2 K. A comparison of T_{EHD} and T_{ex} shows that in this entire interval T_{EHD} is always 2–3 K higher than the exciton temperature. The difference between T_{EHD} and T_{ex} has apparently a definite meaning and is connected with the fact that the EHD contains its own heat "source," due to the intense generation of phonons by electron-hole recombination. In the subsequent discussion of the results, however, we shall neglect the difference between T_{ex} and T_{EHD} , since it barely exceeds the experimental error, and will assume throughout that T_{EHD} is equal to T_{ex} .

Figure 4a shows two plots of $n_0(T)$ measured under conditions of stationary and pulsed excitations at $T < 20$ K. The difference between them reaches 20% at $T = 18$ K, and the question of the cause of this difference still remains open. We note that as this paper was written a communication was published (see^[13]), citing the $n_0(T)$ dependence in silicon only in the interval $2 \text{ K} < T < 13 \text{ K}$. The values of n_0 determined in^[13] agree in this temperature interval with our data for pulsed excitations, with accuracy up to 10%.

2. At $T > 20$ K, the determination of the density n_0 and of the temperature T_{EHD} directly from the shape of the EHD recombination spectrum is an unsurmountably dif-

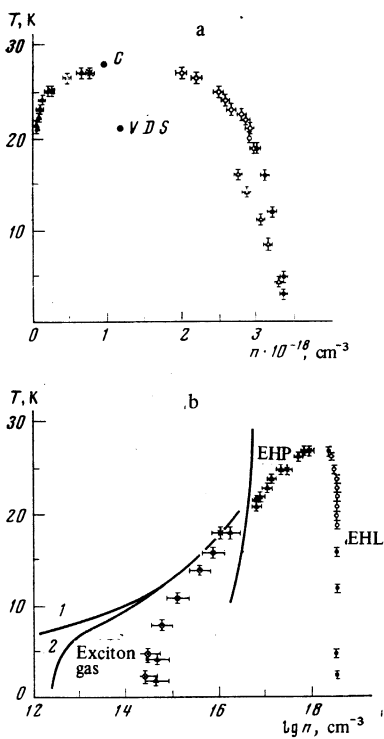


FIG. 4. Phase diagram in nonequilibrium electron-hole system in silicon. The experimental points are determined from the following: the shape of the spectrum under pulsed excitation (PE, ●) and under stationary excitation (SE, Δ), from the red boundaries of the EHD (○) and the EHP (▲) spectra under PE above 20 K, from the threshold of the onset of the EHD under PE (×) and under SE (▲), and from the dependence of the integral intensity of the exciton emission on the temperature under SE (⊗). The points C and VDS were calculated in [16] and [17]. The calculation of the threshold density of the saturated exciton gas n_{ex}^0 in the detailed-balancing approximation is shown by curve 1, and with the aid of Eq. (9) by curve 2. Curve 3—Mott transition line $n_{MT}(T)$.

difficult problem, since in this temperature region the emission spectra of the EHD and of the gas surrounding them overlap to a considerable degree. To determine the function $n_0(T)$ we used the dependence of the spectral transition of the "red" boundary of the EHD band on the carrier density.

The procedure of determining n_0 consisted in the following. For a metallic liquid, the temperature dependences of the contributions to the free energy per pair of particles in EHD connected with exchange and correlation interactions practically cancel each other in the density and temperature regions where the plasma frequency $\omega_p \gg kT/\hbar$ [9] (in silicon we have $\hbar\omega_p \approx 20 \text{ meV} \cdot (n \cdot 10^{-18} \text{ cm}^{-3})^{1/2}$). Assuming that $\Delta\epsilon_{xc}(n_0, T) \approx \Delta\epsilon_{xc}(n_0)$, the change of the position of the "red" boundary can be written in the form

$$\Delta\hbar\omega_r(n_0, T) \approx \Delta E_g(T) + \Delta\epsilon_{xc}(n_0).$$

Next, using the calculations of $\epsilon_{xc}(n_0)$ for silicon in the range of values of the dimensionless parameter r_s from 0.8 to 1, carried out in [14], we plotted a calibration

curve for $\Delta\hbar\omega_r$. To determine n_0 it turned out to be more convenient and more accurate to use the experimental values of the energies $\hbar\omega_{1/2}$ on the long-wave wing of the EHD band, where the intensity of the recombination radiation of the EHD amounted to half the intensity at the maximum. A correction dependent on n_0 and T , was introduced for the difference between $\hbar\omega_{1/2}$ and $\hbar\omega_r$, in conformity with the distribution (3).

Choosing as the reference point the value of n_0 at $T=3 \text{ K}$, as determined from the shape of the EHD spectrum ($n_0(3 \text{ K}) = 3.35 \cdot 10^{18} \text{ cm}^{-3}$), we determined the $n_0(T)$ dependence in the entire range of temperatures of interest to us, $T \lesssim 27 \text{ K}$ (Fig. 4a). In the region $T < 20 \text{ K}$, the $n_0(T)$ dependence obtained in this manner agreed within 1% with that previously determined from the shape of the emission spectrum of the EHD. This agreement, in our opinion, provides another argument in favor of the selected method of determining $n_0(T)$.

It is seen from Fig. 4a that $n_0(T)$ decreases strongly at $T \gtrsim 25 \text{ K}$, thus evidencing an approach to the critical temperature.

5. THERMODYNAMIC CHARACTERISTICS OF ELECTRON-HOLE LIQUID

To describe the temperature dependence of a metallic electron-hole liquid we used, following [9, 15, 16], the Landau theory for a Fermi liquid. The free energy $F(n, T)$ per $e-h$ pair in the region where $kT \ll \epsilon_F^e, \epsilon_F^h$, can be represented in the form of an expansion in powers of the temperature:

$$F(n, T) = \epsilon_0(n) - 1/2 \gamma(n) (kT)^2, \quad (4)$$

where $\epsilon_0(n)$ is the energy of the ground state at $T=0$, $\gamma(n) = (\pi/3n\hbar^3)^{2/3} (m_{de} + m_{dh})$ and m_{de}, m_{dh} , are the effective masses of the densities of state of the electrons (holes) with allowance for the band-degeneracy multiplicity. Equation (4) yields corrections, quadratic in the temperature, to the chemical potential μ_F , to the Fermi energy $E_F = \epsilon_F^e + \epsilon_F^h$, and to the equilibrium density n_0 of the $e-h$ pairs in the liquid phase:

$$\begin{aligned} \mu_F(T) &= \mu_F(0) - \delta_\mu E_F(0) (kT)^2, \quad E_F(T) = E_F(0) [1 - \delta_E (kT)^2], \\ n_0(T) &= n_0(0) [1 - \delta_n (kT)^2], \end{aligned} \quad (5)$$

where

$$\begin{aligned} \delta_\mu &= \frac{1}{2} \frac{\gamma(0)}{E_F(0)}, \quad \delta_n = \frac{1}{2} \frac{\gamma'(0)}{n_0(0) \epsilon_0''(0)}, \\ \delta_E &= \frac{\pi^2}{12} \frac{1}{\epsilon_F^e(0) \epsilon_F^h(0)} - \frac{1}{3} \frac{\gamma'(0)}{n_0(0) \epsilon_0''(0)}, \end{aligned}$$

and the prime denotes differentiation with respect to the concentration.

Figure 5 shows approximations of the temperature dependences of $\mu_F(T)$, $E_F(T)$ and $n_0(T)$ with the aid of expression (5). Good agreement with experiment is observed in the temperature region $T < 22 \text{ K}$. The values of the fit parameters $E_F(0)$, $n_0(0)$, $\mu_F(0)$, δ_μ , δ_E , δ_n , and also the values of the compressibility $\chi = [\epsilon_0''(0) \times n_0^3(0)]^{-1}$ and the binding energy $\varphi(0)$, obtained by least squares from the experimental curves, are listed in

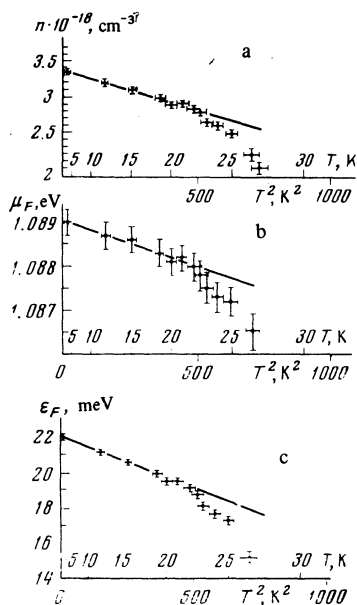


FIG. 5. Approximation of the temperature dependences of the equilibrium density $n_0(T)$, of the Fermi energy $E_F(T)$, and of the chemical potential $\epsilon_F - \hbar\omega^{TO}$ per electron-hole pair in an EHL.

Table I. A theoretical calculation of these parameters for silicon was recently carried out in^[17]. We note that the authors of^[17] have assumed in the calculation of γ that $m_{de} + m_{dh} = 2m_0$ instead of the actual $1.6m_0$.^[18] Therefore the values of δ_n , δ_μ , and δ_B calculated by them are approximately 20% too high. Comparing the experimental data with those calculated in^[17], we can note good agreement for the values of $n_0(0)$, $E_F(0)$, $\varphi(0)$, χ ; however, the experimentally obtained coefficients δ_n , δ_μ , and δ_B turned out to be less than those calculated in^[17] by an approximate factor of two. Accordingly, the critical temperature $T_c = 20.8$ K calculated in^[17] is also appreciably lower than the experimentally estimated value $T_c = (28 \pm 2)$ K (see Sec. 6).

6. GAS-LIQUID EQUILIBRIUM REGION ON THE GAS-PHASE SIDE

1. $T < 18$ K. *Exciton-gas-EHD transition.* For an experimental determination of the thermodynamic gas-liquid coexistence curves on the gas-phase side it is necessary to determine the saturated vapor density of the exciton gas n_{ex}^0 corresponding to the threshold excitation intensity P_{thr} at which the EHD band begins to appear in the recombination radiation spectra. For an estimate of n_{ex}^0 from P_{thr} it was assumed that the exciton diffusion length in the interior of the sample is $100 \mu\text{m}$ and that the surface recombination can be neglected. We note that if the sample surface is carefully finished by chemical polishing, the recombination times under volume and surface excitations are practically the same. The exciton lifetimes τ_{ex} were estimated from the pulsed measurements with accuracy up to 10%. The error in the value of n_{ex}^0 was governed by the correctness of the assumptions made and ranged over one order of magnitude. Thus, at $T = 18$ K the value of n_{ex}^0 estimated in this manner differed by only 1.3 times from

n_{ex}^0 obtained from threshold measurements in the pulsed regime, when a calibration for $\bar{n}(P)$ could be carried out, while the error in the value of n_{ex}^0 was within 20% (see Sec. 6.2 below). The threshold values of n_{ex}^0 were estimated for an experimental situation wherein the ratio of the integrated intensities of the EHD and exciton emission bands was 1 : 15. Only at helium temperatures $T < 5$ K, when the EHD band rises over the background of the lines of the multiparticle exciton-impurity complexes, was the EHD production threshold estimated at an intensity ratio 1 : 1 of the corresponding band. The $n_{ex}^0(T)$ dependence obtained under the conditions of the stationary excitation is shown in Fig. 4b.

An independent method of constructing the $n_{ex}^0(T)$ curve is the measurement of the temperature dependence of the integrated intensity $I_{ex}(T)$ of exciton emission near the threshold of the EHD production. Under conditions when the radiative lifetime of the excitons remains constant at $T < 18$ K, we have $n_{ex}^0(T) \sim I_{ex}(T)$. The $n_{ex}^0(T)$ dependence obtained in this manner is also shown in Fig. 4b (the value of n_{ex}^0 (18 K) was taken from threshold measurements). The agreement between the two methods of determining $n_{ex}^0(T)$ is quite satisfactory. As expected, at low temperatures the experimental $n_{ex}^0(T)$ dependence cannot be described by the expression (see, e.g.,^[11])

$$n_{ex}(T) = g(M_{ex}kT/2\pi\hbar^2)^{3/2} \exp(-\varphi/kT) \quad (6)$$

(Fig. 4b, curve 1), where g is the degeneracy factor of the ground state of the exciton and M_{ex} is the state-density effective mass. Expression (6) is valid under detailed-balancing conditions for nonrecombining particles in a flat gas-liquid interface. Relation (6) agrees with experiment only at $T > 14$ K. This explains the more than threefold discrepancy in the values of the binding energy estimated by the spectroscopic and thermodynamic methods from formula (6) at $T < 12$ K.^[12]

Calculations of the exciton-gas saturated vapor density, in which account is taken of the surface tension, of the finite lifetime of the recombining particles in the EHD, as well as of the diffusion of the excitons in the EHD, yield (see^[19])

$$n_{ex}(T, R) = n_{ex}^* \exp \frac{2\sigma}{n_{ex}RkT} + \frac{n_{ex}R}{3v_T\tau_{ex}} \left(1 + \frac{v_T R}{D} \right), \quad (7)$$

where n_{ex}^* is given by (6), σ is the surface-tension coefficient, v_T is the thermal velocity of the excitons, D is the coefficient of their diffusion, and R is the radius of the EHD. Under the conditions of stationary ex-

TABLE I. Parameters of EHD in silicon.

	Experiment		
	Our data	Data by others	Calculation
$n_0 \cdot 10^{-18}, \text{cm}^{-3}$	3.35 ± 0.05	3.7 [2]; 3.33 [13]	3.2 [17]; 3.4 [18]; 3.1 [16]
$\varphi(0), \text{meV}$	7.9 ± 0.2	8.2 ± 0.1 [15]	7.21 [17]; 5.7 [18]
E_F, meV	22.1	22.1 [15]	21.2 [17]
$\mu_F(0) - \hbar\omega^{TO}, \text{meV}$	1089 ± 0.2	1088.7 ± 0.1 [15]	—
$\delta_n, \text{meV}^{-2}$	0.045 ± 0.01	0.06 ± 0.02 [15]	0.10 [17]
$\delta_\mu, \text{meV}^{-2}$	0.04 ± 0.01	0.05 ± 0.01 [15]	0.078 [17]
$\delta_B, \text{meV}^{-2}$	0.013 ± 0.006	0.036 ± 0.008 [15]	0.024 [17]
$\chi \cdot 10^{10}, \text{eV}^{-1} \cdot \text{cm}^{-3}$	0.7 ± 0.2	—	0.96 [17]
T_c, K	28 ± 2	—	20.8 [17]; 28 [16]
$n_c \cdot 10^{-18}, \text{cm}^{-3}$	1.2 ± 0.2	—	1.2 [17]; 0.8 [16]

citation, as $t \rightarrow \infty$, the values of R and n_{ex} should tend to their limiting values R_0 and n_{ex}^0 determined from the conditions

$$\frac{dn_{\text{ex}}(R_0)}{dR} = 0, \quad (8)$$

$$n_{\text{ex}}^0 = n_{\text{ex}}(R_0). \quad (9)$$

We used formulas (7)–(9) to calculate the $n_{\text{ex}}^0(T)$ dependence for silicon (curve 2 on Fig. 4b). In the calculation, the surface-tension and exciton-diffusion coefficients were assumed to be $\sigma = 3.6 \cdot 10^{-3}$ erg/cm² [20] and $D = 50$ cm²/sec. The calculated curve accounts qualitatively for the measured dependence in the case of $n_{\text{ex}}^0(T)$, but the quantitative discrepancies are large at low temperatures. Moreover, at $T < 5$ K, the EHD radius R_0 estimated with the aid of (8) turned out to be comparable with the Bohr radius of the excitons, obviously a meaningless result. These discrepancies are more readily caused by the fact that expression (7) does not describe the properties of EHD having a small number of particles. The experimental $n_{\text{ex}}^0(T)$ curve is satisfactorily described by expression (7) if we use $R = 0.3$ μm . This value agrees well with the $R \approx 0.75$ μm obtained in [21] by measuring the current pulses connected with the decay of EHD near a $p-n$ junction. We can also note here that although the measurements were made with stationary illumination, the system could still be far from the stationary state described by formulas (8) and (9), owing to the very slow rate of drop production when the exciton gas is not too strongly supersaturated. [19]

It follows also from the determined $n_{\text{ex}}^0(T)$ dependence that the chemical potential of the exciton gas and of the EHD are equal only at $T \gtrsim 15$ K. At low temperatures, when there is no detailed balancing in the system, we have $\mu_{\text{ex}} \neq \mu_{\text{EHD}}$ (for example, $\mu_{\text{ex}} - \mu_{\text{EHD}} = 4$ meV at $T \sim 4$ K).

2. 22 K $< T < 27$ K. EHP-gas-liquid transition. In this temperature region, the study was made only under pulsed excitation of nonequilibrium $e-h$ pairs. The threshold values of the saturated-gas density (EHP), at which the EHD bands begin to appear in the emission spectra (the ratio of the integral intensities of the EHD and EHP bands near the threshold is 1 : 15) were estimated in the following manner.

We determined first the average nonequilibrium $e-h$ pair density corresponding to the maximum pulsed pump. To this end we measured at $T > 30$ K (a temperature higher than critical) the EHP emission spectrum corresponding to the maximum of the excitation pulse. From the position of the “red” limit of the EHP spectrum we then determined \bar{n} in analogy with the determination of the density n_0 for EHD. After such a calibration of the excitation pulse, it was assumed next that $\bar{n} \sim P$. The excitation power was varied with the aid of calibrated filters, and the density n_{EHP}^0 of the saturated EHP gas was then determined from P_{thr} .

The threshold density of the saturated EHP gas can be determined also in an independent manner if one knows the chemical potential μ_{EHP} per pair of particles, and the width $E_g(\bar{n})$ of the forbidden gap, corresponding

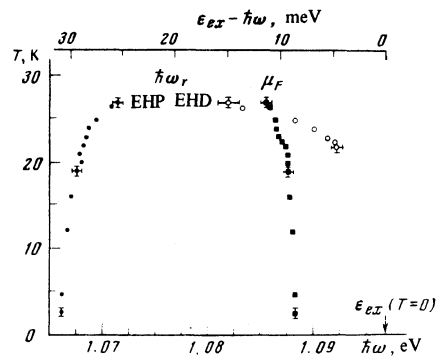


FIG. 6. Temperature dependences of the “red” limits of the recombination radiation spectra and of the chemical potential for EHD and EHP.

to EHP of a given density. The chemical potential of the EHP coincides with μ_{EHD} , and the gap can be determined from the “red” limits of the EHP emission spectra plotted with a delay corresponding to the instant of vanishing of the EHD band. ($\hbar\omega_r$ of the EHP was assumed to be the frequency at which the intensity of the emission was 1/10 of the maximum.) The plots of $n_{\text{EHP}}^0(T)$ obtained by these two independent methods in the interval 22 K $< T < 27$ K are shown in Fig. 4b. The agreement between these plots confirms the assumption that the gas surrounding the EHD is plasma-like in this temperature region.

Figure 6 illustrates the temperature dependences of the chemical potential μ_F , as well as of the “red” end-points of the EHD and EHP spectra, measured along the gas-liquid equilibrium curves. The “red” limits $\hbar\omega_r$ of the EHP and EHD correspond, within the framework of the considered approximations, to the corresponding widths of the forbidden gaps E_g' . It is seen here that the EHP produced as a result of “metallization” of the dielectric exciton gas at $\bar{n} \sim 5 \times 10^{16}$ cm⁻³ remains a non-degenerate gas surrounding the EHD up to $\bar{n} \sim 3 \times 10^{17}$ cm⁻³ ($T = 26$ K). The recombination radiation band of the degenerate EHP ($\bar{n} > 5 \times 10^{17}$ cm⁻³) overlaps strongly the EHD emission line. In the immediate vicinity of the critical temperature, the contours of the EHD and EHP bands can therefore not be separated in principle either by the spectral positions of these bands or by the kinetics of their shapes. The determination of the critical parameters n_c and T_c directly from the recombination radiation spectra is therefore impossible. The values of the critical temperature and density can be estimated only by extrapolating the $n_0(T)$ and $n_{\text{EHP}}^0(T)$ curves. This extrapolation yields $n_c = (1.2 \pm 0.2) \times 10^{18}$ cm⁻³ and $T_c = (28 \pm 2)$ K. These values agree well with the $n_c = 0.8 \times 10^{18}$ cm⁻³ and $T_c = 28$ K calculated in [16].

In conclusion, the authors thank L. V. Keldysh, Ya. E. Pokrovskii, and T. G. Tratas for useful discussions, and S. I. Gubarev for a number of computer calculations.

¹L. V. Keldysh, in: Eksitony v poluprovodnikakh (Excitons in Semiconductors), Nauka, 1971, p. 5.

²R. B. Hammond, D. L. Smith, and T. C. McGill, Phys. Rev.

- Lett. **35**, 1535 (1975).
- ³N. V. Alkeev, A. S. Kaminskiĭ, and Ya. E. Pokrovskii, *Fiz. Tverd. Tela (Leningrad)* **17**, 843 (1975) [*Sov. Phys. Solid State* **17**, 535 (1975)].
- ⁴K. Kozai and M. Gershenson, *Phys. Rev.* **B9**, 723 (1974).
- ⁵R. B. Hammond, T. C. McGill, and J. W. Mayer, *Phys. Status Solidi A* **33**, 59 (1976).
- ⁶B. M. Ashkinadze, I. P. Kretsu, S. M. Ryvkin, and I. D. Yaroshetskii, *Zh. Eksp. Teor. Fiz.* **58**, 507 (1970) [*Sov. Phys. JETP* **31**, 264 (1970)].
- ⁷A. F. Dite, V. G. Lysenko, and V. B. Timofeev, *Phys. Status Solidi B* **66**, 53 (1974).
- ⁸F. I. Rogers, H. C. Graboski, and D. J. Harwood, *Phys. Rev. A* **1**, 1577 (1970).
- ⁹T. M. Rice, *Proc. Twelfth Intern. Conf. on Physics of Semiconductors, Stuttgart, 1974*, publ. by Teubner, Stuttgart (1974), p. 23.
- ¹⁰G. E. Horman and A. N. Starostin, *Teplofiz. Vys. Temp.* **8**, 413 (1970).
- ¹¹W. D. Kraeft, K. Kilimann, and D. Kremp, *Phys. Status Solidi B* **72**, 461 (1975).
- ¹²A. S. Kaminskiĭ, Ya. E. Pokrovskii, and N. V. Alkeev, *Zh. Eksp. Teor. Fiz.* **59**, 1937 (1970) [*Sov. Phys. JETP* **32**, 1048 (1971)].
- ¹³R. B. Hammond, T. C. McGill, and J. W. Mayer, *Phys. Rev.* **B8**, 3566 (1976).
- ¹⁴P. Bhattacharyya, V. Nassida, K. S. Singwi, and P. Vashishta, *Phys. Rev.* **B10**, 5127 (1974).
- ¹⁵G. A. Thomas, T. G. Phillips, T. M. Rice, and J. C. Hensel, *Phys. Rev. Lett.* **31**, 386 (1973).
- ¹⁶M. Combescot, *Phys. Rev. Lett.* **32**, 15 (1972).
- ¹⁷P. Vashishta, S. G. Das, and K. S. Singwi, *Phys. Rev. Lett.* **33**, 911 (1974).
- ¹⁸W. F. Brinkman and T. M. Rice, *Phys. Rev.* **B7**, 1508 (1973).
- ¹⁹V. S. Bagaev, N. V. Zamkovets, L. V. Kelsysh, N. N. Sibel'din, and V. A. Tsvetkov, *Zh. Eksp. Teor. Fiz.* **70**, 1501 (1976) [*Sov. Phys. JETP* **43**, (1976)].
- ²⁰T. L. Reinecke and S. C. Ying, *Phys. Rev. Lett.* **35**, 311 (1975).
- ²¹M. Capizzi, M. Voos, C. Benoit a la Guillaume, and J. C. McGroddy, *Solid State Commun.* **16**, 709 (1975).

Translated by J. G. Adashko

Laser induced breakdown of alkali-halide crystals

B. G. Gorshkov, Yu. K. Danileiko, A. S. Epifanov, V. A. Lobachev, A. A. Manenkov, and A. V. Sidorin

P. N. Lebedev Physics Institute, USSR Academy of Sciences
(Submitted September 1976)
Zh. Eksp. Teor. Fiz. **72**, 1171-1181 (March 1977)

The frequency and temperature dependences of the laser-induced breakdown thresholds of a number of alkali halide crystals are investigated. In the samples with the highest thresholds the dependences agree qualitatively with the avalanche ionization theory and this mechanism is the probable cause of their destruction. Possible causes of the quantitative discrepancy between theory and experiment are discussed.

PACS numbers: 79.20.Ds, 77.50.+p

1. INTRODUCTION

The mechanism of laser-induced breakdown of solid transparent dielectrics remains to this day a complicated and debatable problem in the physics of the interaction between high-power electromagnetic radiation and matter. For pure materials, in the case of pulses in the picosecond range, the most widely discussed mechanism is the electron avalanche due to impact ionization.^[1] It is still unclear, however, whether this mechanism predominates in the breakdown of real materials, since the latter always contain various kinds of defects and inclusions that can influence strongly the breakdown process.

It was stated in^[2-5] that the electron-avalanche mechanism was realized in the alkali-halide crystals investigated by the authors. The proof advanced in the cited papers, however, can hardly be regarded as convincing. In fact, the statements there were based mainly on the following observed experimental facts: a) the independence of the laser-breakdown threshold of the frequency

in a wide range, and the fact that these thresholds agreed with those observed in constant electric fields; b) the correlations of the thresholds in the series of the alkali-halide crystals. It was also stated that no effects of the absorbing inclusions were accounted for in the experiments. All this, however, cannot be regarded as fully convincing proof in the favor of a breakdown mechanism that is connected with the development of an electron avalanche. In fact:

1. The independence of the thresholds of the frequency may also be a property of other breakdown mechanisms, including the thermal one. And if this fact is analyzed within the framework of the electron avalanche mechanism, then it means that the relaxation time τ of the longitudinal component of the momentum of the "hot" electrons turns out to be shorter than 6×10^{-16} sec, which is, in the very least, unexpected and requires careful corroboration. The comparison that was carried out between the thresholds of laser breakdown and